Time-Resolved Fluorescence Studies of Heterotropic Ligand Binding to Cytochrome P450 3A4†

Jed N. Lampe and William M. Atkins*

Department of Medicinal Chemistry, Box 357610, University of Washington, Seattle, Washington 98195-7610

Received January 13, 2006; Revised Manuscript Received August 17, 2006

ABSTRACT: Cytochrome P450 3A4 (CYP3A4) is a major enzymatic determinant of drug and xenobiotic metabolism that demonstrates remarkable substrate diversity and complex kinetic properties. The complex kinetics may result, in some cases, from multiple binding of ligands within the large active site or from an effector molecule acting at a distal allosteric site. Here, the fluorescent probe TNS (2-*p*-toluidinylnaphthalene-6-sulfonic acid) was characterized as an active site fluorescent ligand. UV−vis difference spectroscopy revealed a TNS-induced low-spin heme absorbance spectrum with an apparent K_d of 25.4 ± 2 μM. Catalytic turnover using 7-benzyloxyquinoline (7-BQ) as a substrate demonstrated TNS-dependent inhibition with an IC_{50} of 9.9 ± 0.1 μM. These results suggest that TNS binds in the CYP3A4 active site. The steady-state fluorescence of TNS increased upon binding to CYP3A4, and fluorescence titrations yielded a K_d of 22.8 ± 1 μM. Time-resolved frequency-domain measurement of TNS fluorescence lifetimes indicates a testosterone (TST)-dependent decrease in the excited-state lifetime of TNS, concomitant with a decrease in the steady-state fluorescence intensity. In contrast, the substrate erythromycin (ERY) had no effect on TNS lifetime, while it decreased the steady-state fluorescence intensity. Together, the results suggest that TNS binds in the active site of CYP3A4, while the first equivalent of TST binds at a distant allosteric effector site. Furthermore, the results are the first to indicate that TST bound to the effector site can modulate the environment of the heterotropic ligand.

The heme-containing hepatic and intestinal cytochrome P450s (CYPs)[1] control the metabolism of most toxins and drugs (*1*−*3*). CYP3A4 is the major component of CYP-dependent clearance, although others also contribute. An emerging paradigm concerning these microsomal CYPs is their tendency to exhibit complex non-Michaelis−Menten kinetic profiles in vitro. Although the extent of in vivo allosteric kinetics remains in question, the in vitro complexity hinders the practical prediction of clinical outcomes based on in vitro experiments. Both homotropic and heterotropic effects have been well documented (*4*−*9*). This allosteric behavior appears to result from the simultaneous binding of multiple drugs to a single CYP. Recently, published crystal structures of several CYPs, including CYP3A4, suggest that the active site is sufficiently large to accommodate multiple ligands (*10*, *11*).

It has been difficult to determine the spatial relationship of various ligand binding sites within the CYP3A4 scaffold by steady-state kinetic methods. Thus, it remains unknown whether homotropic and heterotropic interactions occur because of simultaneous binding by multiple ligands within the large active site or due to remote, spatially distinct binding sites. For example, an effector ligand could bind to peripheral sites on the protein surface and alter the kinetic properties of substrates within the active site via long-range effects. A crystal structure of the [CYP3A4·progesterone] complex indicates that the steroid is not bound at the active site but rather lies in a hydrophobic patch near the protein surface, known as the "phenylalanine cluster" due to the propensity of phenylalanine residues at this location (*11*). Alternatively, the effector could bind within the active site and directly alter the active site physical properties such as volume, hydration, and hydrogen bonding (*12*). Furthermore, both scenarios may be relevant, depending on the specific combination of ligands. Clearly, new methods are required to efficiently distinguish between the possible mechanisms of allosterism for a wide range of ligand combinations.

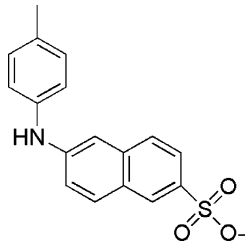

FIGURE 1: Structure of 2-*p*-toluidinylnaphthalene-6-sulfonic acid (2,6-TNS).

Here we report results from steady-state and frequency domain fluorescence lifetime measurements using TNS as a probe (Figure 1). The unique photophysical properties of TNS result in a nonfluorescent compound in aqueous

† This work was supported by NIH Grants GM32165 (W.M.A.) and GM07750 (J.N.L.).

* To whom correspondence should be addressed. E-mail: winky@u.washington.edu. Telephone: (206) 685-0379. Fax: (206) 685-3252.

[1] Abbreviations: CYP, cytochrome P450; TNS, 2-*p*-toluidinylnaphthalene-6-sulfonic acid; ANS, 1-anilino-8-naphthalenesulfonic acid; TST, testosterone; 7-BQ, 7-benzyloxyquinoline; 7-HQ, 7-hydroxyquinoline; ERY, erythromycin; Trp, tryptophan; POPOP, 1,4-bis(4-methyl-5-phenyloxazol-2-yl)benzene.

10.1021/bi060083h CCC: $33.50
Published on Web 09/16/2006

solution, but with a high quantum yield when bound to hydrophobic regions of a protein such as the CYP3A4 active site. Therefore, we concluded that TNS should function well as a probe for direct assessment of binding of a ligand to CYP3A4. The results obtained here from UV−vis titrations indicate that TNS binds within the active site. Moreover, data with TNS binding in the presence of testosterone (TST) demonstrate that the highest-affinity TST binding site is remote from the protoporphyrin heme. Together, these results support previous evidence for a TST binding site distant from the heme iron (*13*), and they provide the first indication that TST modulates the environment of the active site from its high-affinity effector site.

MATERIALS AND METHODS

Chemicals. All chemicals were analytical grade and obtained from commercial sources. The potassium salt of 2-*p*-toluidinylnaphthalene-6-sulfonic acid (TNS) was obtained from Marker Gene Technologies (Eugene, OR). Testosterone was obtained from Steraloids (Newport, RI). Erythromycin and all other chemicals used were obtained from Sigma-Aldrich (St. Louis, MO), unless otherwise noted.

Protein Expression and Purification. Recombinant CYP3A4 was expressed and purified from *Escherichia coli* as described previously, except that a French press was used to lyse the cells (*14*). To ensure complete lysis, cells were passed twice through a French pressure cell (Thermo IEC, Needham Heights, MA) at 10 000 psi. When purification was complete, the concentration of CYP3A4 was quantified by the method of Omura and Sato, using an extinction coefficient of 91 mM^{-1} cm^{-1} (*15*). The protein was judged to be greater than 95% pure by SDS−PAGE. The purified CYP3A4 was divided into 1 mL aliquots and stored at −80 °C until further use. Each aliquot underwent no more than five freeze−thaw cycles.

Determination of IC_{50} Values for TNS Inhibition. IC_{50} values were determined according to the method of Cheng and Prusoff (*16*), using a reconstituted enzyme system as described previously (*17*). The CYP3A4-mediated O-debenzylation of 7-benzyloxyquinoline (7-BQ) was monitored as a function of TNS concentration. Steady-state emission spectra were recorded to ensure no interference from background TNS fluorescence. Reconstituted enzyme mixes were incubated with a substrate concentration equivalent to the K_m of the substrate (70 μM for 7-BQ) (*18*) and TNS (concentration range of 0−200 μM) under the conditions described previously (*17*). Briefly, 30 pmol of purified CYP3A4, 60 pmol of rat NADPH-P450 reductase, and 30 pmol of rat cytochrome b_5 were resuspended in a buffer containing 0.1 mg/mL CHAPS, 20 μg/mL liposomes [L-α-dilauroyl-*sn*-glycerophosphocholine, L-α-dioleoyl-*sn*-glycero-3-phosphocholine, L-α-dilauroyl-*sn*-glycero-3-phosphoserine, at a 1:1:1 (w/w/w) ratio per milliliter], 600 μM GSH, and 10 mM potassium HEPES (pH 7.4). Reaction buffer and MilliQ NanoPure H_2O were added to a final concentration of 40 mM potassium HEPES (pH 7.4), 2.4 mM GSH, and 30 mM $MgCl_2$. This enzyme mixture was then allowed to preincubate on ice for 10 min. Reaction mixtures were then preincubated at 37 °C for 5 min, after which the reaction was initiated by addition of 1 mM NADPH. The final reaction volume was 1 mL. The reaction was allowed to proceed for 10 min at 37 °C, at which time product formation was assessed using an AB2 SLM-Aminco luminescence spectrometer set at an excitation wavelength of 409 nm and an emission wavelength of 530 nm with a band-pass of 4 nm for both wavelengths. The photomultiplier tube was set to 550 V. A (−) NADPH control was completed for each sample to correct for background fluorescence. Since the formation of 7-hydroxyquinoline (7-HQ) by CYP3A4 was determined to be linear over an incubation period of 20 min under these conditions, an incubation time of 10 min was employed for all kinetic determinations. Product formation was calculated by comparison to a standard curve for 7-HQ fluorescence and converted to nanomoles per minute per nanomole of CYP3A4. IC_{50} values for TNS inhibition were determined by fitting the data using GraphPad Prism (GraphPad Software, San Diego, CA) to the variable slope sigmoidal dose−response equation (eq 1):

$$v = \frac{100}{1 + 10^{B(\log IC_{50} - [I])}} \quad (1)$$

where B is a factor that varies the slope of the curve to achieve the best fit.

TNS K_d Determination using Optical Difference Spectroscopy. To determine the equilibrium binding constant (K_d) for binding of TNS to CYP3A4, UV−visible difference spectra were acquired using a single-beam Agilent (Palo Alto, CA) model 8453 UV−vis spectrophotometer. Because of the strong UV absorbance of TNS below 380 nm, spectra were obtained using the absolute difference method, as described previously (*13*). The instrument was referenced against a buffer containing 100 mM KP_i (pH 7.4), 10% glycerol, and 1 mM EDTA. Subsequently, an initial spectrum was obtained for a 1 mL solution of 1 μM 3A4 diluted into the same buffer. The titration was begun by adding 1 μL aliquots of 1 mM TNS dissolved in 50% ethanol to the cuvette and recording the full spectrum after a 1 min equilibration time. The titration continued until the peak at ∼425 nm reached apparent saturation (∼30 μM TNS). At the conclusion of the titration, the final concentration of ethanol did not exceed 1.5%. However, to take into account any possible effect of solvent on the heme spin state, this titration was normalized to a separate control titration of CYP3A4 conducted with ethanol to a final concentration of 1.5%. All spectra were recorded at 22 °C (room temperature). After the initial spectrum was subtracted from each subsequent spectrum, a K_d value for the binding of TNS was obtained by comparing the absolute change in absorbance in the peak at 425 nm versus the trough at 398 nm and fitting these values to the Michaelis−Menten equilibrium binding equation (eq 2):

$$\frac{\Delta ABS}{ABS_{max}} = \frac{[S]}{K_d + [S]} \quad (2)$$

using Origin version 7.5 (OriginLab Corp., Northampton, MA).

Competitive Ligand Displacement Experiments. For the competitive ligand displacement experiments, UV−visible difference spectra were acquired using a dual-beam OLIS/Aminco DW2a spectrophotometer (OLIS, Bogart, GA). For each titration with a competitive ligand, the sample chamber contained a 1 mL volume of 5 μM 3A4 in 100 mM KP_i (pH

7.4), 10% glycerol, and 1 mM EDTA. The reference chamber contained only 100 mM KP_i (pH 7.4), 10% glycerol, and 1 mM EDTA. A baseline was recorded between 350 and 500 nm. TNS was added to the sample cuvette to a final concentration of 3 μM, and an initial difference spectrum was recorded. Subsequently, a 10 mM stock concentration of competitive ligand (either TST or ERY dissolved in 50% ethanol) was added in 1 μL aliquots to both the sample and the reference cuvette, and difference spectra were recorded after a 1 min equilibration time. Care was taken so that the final concentration of ethanol did not exceed 1.5%. All spectra were recorded at 22 °C (room temperature).

*Steady-State Fluorescence Spectroscop*y. All steady-state fluorescence measurements were carried out using an AB2 SLM-Aminco luminescence spectrofluorometer with both emission and excitation monochromators. For binding titrations with TNS, the excitation wavelength was 318 nm and the emission wavelength was 443 nm with a band-pass of 4 nm for both monochromators. Emission spectra were acquired from 350 to 600 nm at a rate of 5 nm/s. The potassium salt of TNS was dissolved in a solution of 50% ethanol, and the titrations were carried out as described above for measurement of the UV−vis difference spectra. To determine the extent of binding, the total fluorescence area under the curve from 375 to 600 nm was integrated and the data were fit to eq 2 using Origin version 7.5. For the steady-state tryptophan quenching experiments, Trp residues in 3A4 were excited at 295 nm and emission was monitored from 300 to 550 nm. Titrations with TST or ERY were carried out as described above with the TNS ligand at a concentration of 3 μM, and each ligand dissolved in 50% ethanol, with constant stirring between additions. For each titration, a CYP3A4 concentration of 5 μM in 100 mM KP_i (pH 7.4), 10% glycerol, and 1 mM EDTA was titrated with ligand such that the additions did not exceed more than 1.5% of the final volume. To determine the extent of competitive ligand binding by displacement and dynamic quenching, the amount of quenching for each ligand concentration was converted into a percentage of the total and the data were fit to the quadratic binding equation used previously for binding of multiple ligands to CYP3A4 (*13*) (eq 3):

$$[\text{CYP}\cdot\text{L}\cdot\text{L}] = \{[\text{CYP3A4}]_T[\text{L}]^2/(\alpha K_d)^2\}/[1 + [\text{L}]/K_d + [\text{L}]^2/(\alpha K_d)^2] \quad (3)$$

where L is TST in the case of testosterone and α is a scaling factor that relates the K_d values of the distinct binding events (*13*). Equation 2 was used in the case of binding of ERY to CYP3A4. Data were fit using Origin version 7.5.

Fluorescence Lifetime Measurements. Fluorescence lifetime measurements were conducted using a Spex Fluorolog Tau3 frequency domain spectrofluorometer with a 450 W xenon arc lamp (Horiba Jobin Yvon, Edison, NJ). For each experiment, a total of 20 frequencies were chosen, ranging from 1 to 200 MHz. Ten replicate measurements were obtained for each frequency, and the integration time for each measurement was 15 s. For the TNS lifetime experiments, the excitation monochromator was set at 318 nm and the emission monochromator was set at 440 nm. For the tryptophan lifetime experiments, the excitation monochromator was set at 295 nm and the emission at 330 nm. POPOP was used as an internal lifetime standard for the TNS experiments, whereas *p*-terphenyl was used as an internal lifetime standard for the tryptophan experiments (*19*). Titration experiments were carried out in a manner identical to that of the steady-state experiments (see above). All experiments were performed at 15 °C. Phase angle shift (φ) and modulation (m) decay data were fit to the simplest exponential decay model using the Model software package (Thermogalactic, Waltham, MA), according to the following intensity decay law (eq 4):

$$I(t) = \sum_{i=1}^{n} \alpha_i \exp(-\tau/\tau_i) \quad (4)$$

where α_i is the time-zero amplitude due to each specific decay time (τ_i). In terms of a single-exponential decay, the lifetime can be calculated from the phase and modulation values using

$$\tau_\varphi = \omega^{-1} \tan \phi \quad (5)$$

$$\tau_m = \omega^{-1}\left(\frac{1}{m^2} - 1\right)^{-1/2} \quad (6)$$

where ω is the light modulation frequency in radians per second, τ_φ is the apparent phase angle shift lifetime, and τ_m is the apparent modulation lifetime. Average lifetimes ($\bar{\tau}$) of multiexponential decay were calculated using eq 7:

$$\bar{\tau} = \sum_{i=1}^{n} \frac{\alpha_i \tau_i^2}{\alpha_i \tau_i} \quad (7)$$

Kinetic Simulations. Kinetic simulations were performed using the GEPASI Biochemical Simulation Module (*20*−*22*) based on the sequential-ordered binding model (eq 3), as described previously for CYP3A4 (*13*).

RESULTS

General Experimental Design. The goal of these studies was to determine whether time-resolved fluorescence methods could be used to distinguish between "allosteric" ligand interactions and simple competitive ligand interactions. Therefore, several of the experiments were performed at subsaturating concentrations of the major probe used here, TNS. This experimental design minimizes the likelihood of multiple TNS molecules binding on a single CYP3A4 molecule and, thus, simplifies the spectroscopic interpretation: only a single fluorescent species, [CYP3A4·TNS], is affected by subsequent addition of a heterotropic ligand. A shortcoming of this design is that it decreases sensitivity by limiting the concentration of the reporter species, and it also introduces thermodynamic complexity into the heterotropic interaction studies, wherein several species compete for the heterotropic ligand. For example, with TST as a heterotropic ligand, and assuming at least two TST molecules can bind, free [CYP3A4], [CYP3A4·TNS], and [CYP3A4·TST] may all compete for added TST. This precludes determination of true K_d values for the heterotropic ligand and quantitative analysis of the energetics of cooperativity with the experimental design used here. The ligand affinities reported here for TST are "apparent" K_d values only, as described within.

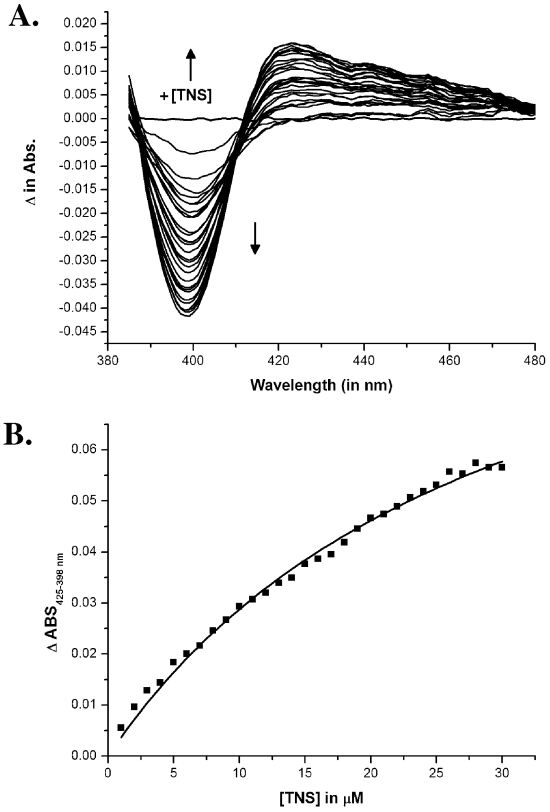

FIGURE 2: TNS is a low-spin ligand of CYP3A4. (A) UV−vis difference spectra of binding of TNS to CYP3A4. Aliquots (1 μL) of a solution of 1 mM TNS were added to a cuvette containing 1 μM CYP3A4. Each spectral scan represents one addition. The arrow designates increasing TNS concentration. The spectra suggest that a low-spin complex is formed. (B) Binding isotherm for TNS based on the optical spectra in the top panel. The difference in absorbance ($A_{425} - A_{398}$) was used, and the data were fit to eq 2 to yield a K_d of 25.4 ± 2.09 μM.

Binding of TNS to CYP3A4. While screening a panel of established fluorescent probes, we observed that TNS (Figure 1) afforded a spectral change consistent with perturbation of CYP3A4 to the low-spin ferric heme. UV−vis difference spectra at multiple concentrations of TNS are shown in Figure 2A. The data clearly indicate that TNS perturbs the immediate environment of the heme iron, affording a type II spectrum, resulting in an increase in the fraction of low-spin heme. Fitting of the titration data to eq 2 yielded a K_d of 25.4 ± 2.09 μM. Due to the limited solubility of TNS in the buffer used, complete saturation was not achieved. However, with 30 data points the range of TNS concentrations used can be fit with reasonable confidence to a Michaelis−Menten equilibrium binding equation (Figure 2B). In addition, TNS was studied as a possible inhibitor of CYP3A4 by monitoring 7-BQ metabolism at varying concentrations of TNS. A clear concentration-dependent inhibition of 7-BQ metabolism was observed with a recovered IC_{50} of 9.9 ± 0.1 μM, thus demonstrating that TNS is a potent inhibitor of CYP3A4 (Figure 3). The IC_{50} value and the K_d values are in reasonable agreement, even though the solution conditions for binding of TNS and inhibition of catalysis by TNS were different. The catalytic studies included reductase, cytochrome b_5, and required detergents, which are not present in the fluorescence studies. The most likely scenario consistent with the optical titrations and inhibition data is that TNS binds in the active site and ligates directly to the heme

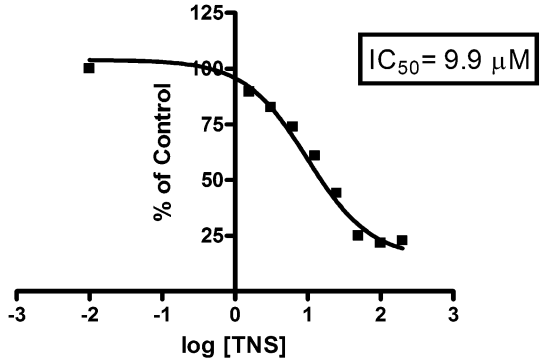

FIGURE 3: Inhibition of catalytic turnover by TNS using 7-BQ as a substrate. The IC_{50} obtained from fitting the data to eq 1 is 9.9 ± 0.1 μM.

iron. The only other possibility, that a protein residue ligates the heme iron and yields a type II spectrum, has, to our knowledge, never been observed with CYP3A4. Presumably, the low-spin spectrum reflects direct TNS−heme ligation.

TNS Fluoresces When It Is Bound to CYP3A4. The fluorescence of TNS in aqueous solution is highly quenched, but the quantum yield increases in nonpolar environments such as hydrophobic protein binding sites (*23*−*26*). On the basis of this well-established behavior, TNS was considered as a potential probe wherein the binding to CYP3A4 would specifically enhance the fluorescence. Figure 4A demonstrates the increase in the steady-state fluorescence spectral intensity of TNS when its is titrated into a solution of CYP3A4. When the integrated steady-state fluorescence signal for each TNS concentration was plotted and fit to eq 2, an apparent K_d of 22.8 ± 1.18 μM was recovered (Figure 4B), consistent with the value obtained from the optical difference spectrum.

Tryptophan Fluorescence Lifetime Measurements. A further probe of interaction of TNS with CYP3A4 is available from the intrinsic protein Trp fluorescence. Upon titration of CYP3A4 with TNS, the steady-state Trp fluorescence decreases (Figure 5A). This may be due to FRET with Trp acting as a donor and TNS as an acceptor, or it may be due to a TNS-induced conformational change of the Trp environments. To further examine this, time-resolved multifrequency phase modulation fluorescence spectroscopy was used to monitor the TNS-dependent decrease in the excited-state lifetime of the tryptophan residues for CYP3A4. Phase modulation data in the absence and presence of 10 μM TNS are shown in Figure 5B. The data were fit to several sum-of-exponential models, and the best fits were obtained with three discrete lifetimes in the absence of TNS and two discrete lifetimes in the presence of TNS (Table 1). Presumably, the lifetime heterogeneity in the ligand-free CYP reflects ground-state heterogeneity and multiple Trp environments, as in other proteins. In the presence of a subsaturating concentration of TNS, additional heterogeneity may be expected due to contributions from both [CYP3A4] and [CYP3A4·TNS]. It is, therefore, very striking that the addition of TNS reduces the number of lifetime components required to fit the data. In the absence of TNS, a small fraction (low α) of a component with a long lifetime is present (10 ns), and this is not observed upon addition of TNS. Regardless of the sources of heterogeneity, which is nearly universally observed for Trp fluorescence, these data

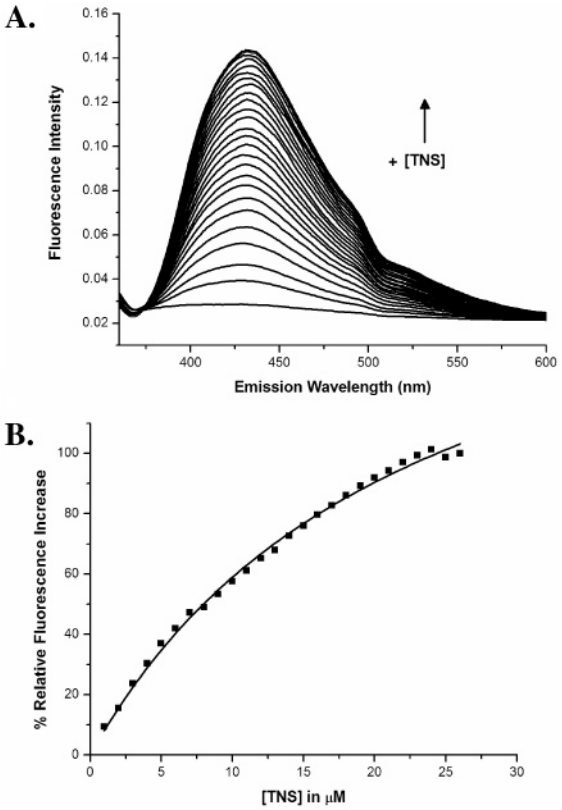

FIGURE 4: TNS fluorescence increases when TNS is bound to CYP3A4. (A) Steady-state emission spectrum of binding of TNS to CYP3A4 with direct excitation of TNS ($\lambda_{ext} = 318$ nm). Aliquots (1 μL) of a solution of 1 mM TNS were added to a cuvette containing 1 μM CYP3A4. Each spectral scan represents one addition. The arrow designates increasing TNS concentration. TNS does not fluoresce significantly in the absence of CYP3A4. (B) Binding isotherm for TNS based on the fluorescence spectra in panel A. To determine the extent of binding, for each titration point the total fluorescence area under the curve from 375 to 600 nm was integrated, and the data were plotted as a function of TNS concentration and fit to eq 2 to yield a K_d of 22.8 $\pm$ 1.18 μM.

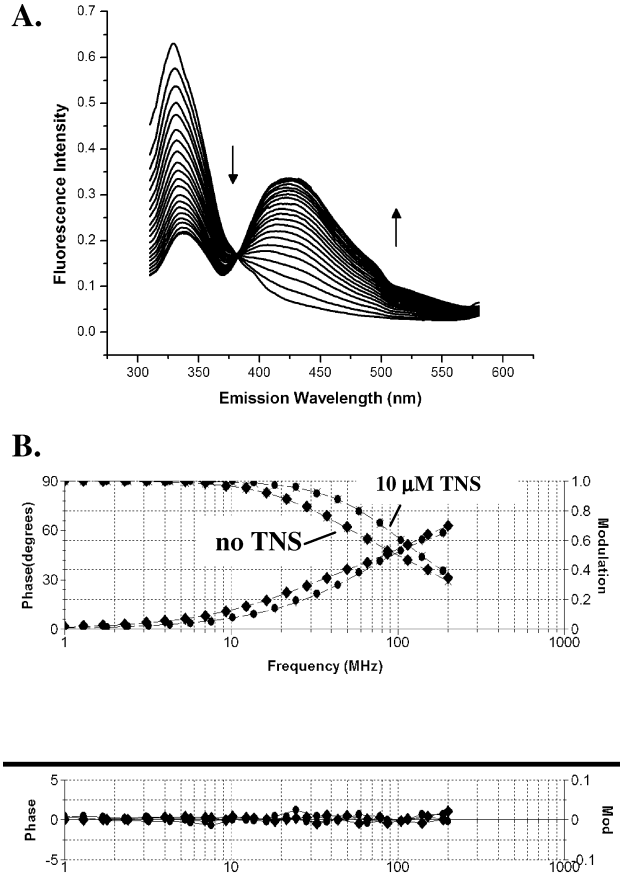

FIGURE 5: TNS quenches tryptophan fluorescence emission and decreases the tryptophan average lifetime. (A) Tryptophan emission spectrum of CYP3A4 when it is excited at 295 nm. Increasing concentrations of TNS quench emission from tryptophan while emission from TNS increases. (B) Phase modulation data for tryptophan emission from 5 μM CYP3A4 in the presence (●) and absence (■) of 10 μM TNS. Note the clear dependence of fluorescence lifetime on TNS concentration.

suggest a TNS-induced change in the environment for at least one of the Trp residues present in CYP3A4, at low TNS occupancy.

Time-Resolved Fluorescence of TNS. The excited-state decay of TNS bound to CYP3A4 was determined by frequency modulation time-resolved fluorescence, using 20 frequencies ranging from 1 to 200 MHz, and multiple wavelengths. Several multiexponential decay models were compared and the data fit best to a three-component model with lifetime values near 0.3, 0.6, and 7.4 ns. The recovered parameters are included in Table 2. Only the results for the 440 nm emission are tabulated. A notable feature of the results is the recovery of a significant negative pre-exponential term at all wavelengths for the short lifetime component, but with an increased magnitude at longer wavelengths. Similar behavior has been reported with TNS and many TNS analogues, such as the related 1-anilino-8-naphthalenesulfonic acid (ANS), when in viscous solvents or bound to proteins (*25*). The negative pre-exponential terms result from an excited-state reaction, as reported previously with this compound (*25*).

Heterotropic Effects between TNS and Testosterone. On the basis of the conclusion that TNS binds at the active site of CYP3A4, its fluorescence properties can be used as a mechanistic probe of heterotropic interactions with other ligands. TST is a well-studied substrate for CYP3A4 and is known to exhibit homotropic and heterotropic behavior (*13*, *27*). With reconstituted CYP3A4, TST exhibits complex biphasic binding, with two or three TST molecules binding each CYP3A4 molecule, possibly depending on whether the enzyme is partially aggregated or monodisperse in nanodisks (*27*−*30*). On the basis of optical difference spectra of the heme spin state and EPR, we previously observed two apparent K_d values of ~22 and ~440 μM for binding of TST to CYP3A4 (*13*). TST binding at the high-affinity site does not perturb the heme spin state (*31*) and thus is likely to be in a remote corner of the active site or at a distinct peripheral site. Therefore, we examined the effects of varying the concentration of TST on the steady-state spectrum and on the fluorescence lifetime of CYP3A4-bound TNS. Figure 6A demonstrates that TNS fluorescence is quenched upon addition of TST and blue-shifted, thus demonstrating a heterotropic ligand effect. The TST concentration dependence of the TNS quenching exhibits complex behavior, consistent with multiple TST molecules binding. In fact, the steady-state quenching curve fits well to a model describing two TST binding sites (eq 3) with apparent K_d values of 14 and 243 μM (Figure 6C), which is in good agreement with the biphasic binding observed previously with heme absorbance and EPR spectra (*13*). It should be noted, as above, that the

Table 1: Excited-State Parameters for Trp Decay in CYP3A4 at 330 nm

[TNS] (μM)	τ_1 (ns)	τ_2 (ns)	τ_3 (ns)	α_1	α_2	α_3	χ^2	$\bar{\tau}^a$ (ns)
0	1.182 ± 0.059	4.665 ± 0.233	10.762 ± 0.538	0.424	0.544	0.031	0.613	4.75 ± 0.238
10	1.060 ± 0.053	4.501 ± 0.225		0.751	0.249		0.710	3.07 ± 0.154

[a] $\bar{\tau} = \sum_{i=1}^{n} \alpha_i\tau_i^2/\alpha_i\tau_i$.

Table 2: Excited-State Parameters for TNS Bound to CYP3A4 with Varying TST Concentrations at 440 nm

[TST] (μM)	τ_1 (ns)	τ_2 (ns)	τ_3 (ns)	α_1	α_2	α_3	χ^2	$\bar{\tau}$ (ns)
0	0.307 ± 0.015	0.608 ± 0.030	7.42 ± 0.371	−0.693	0.969	0.725	0.551	6.98 ± 0.349
20	0.331 ± 0.017	3.418 ± 0.171		0.161	0.839		0.701	3.36 ± 0.168
100	0.576 ± 0.028	2.981 ± 0.149		0.629	0.371		0.606	2.38 ± 0.119

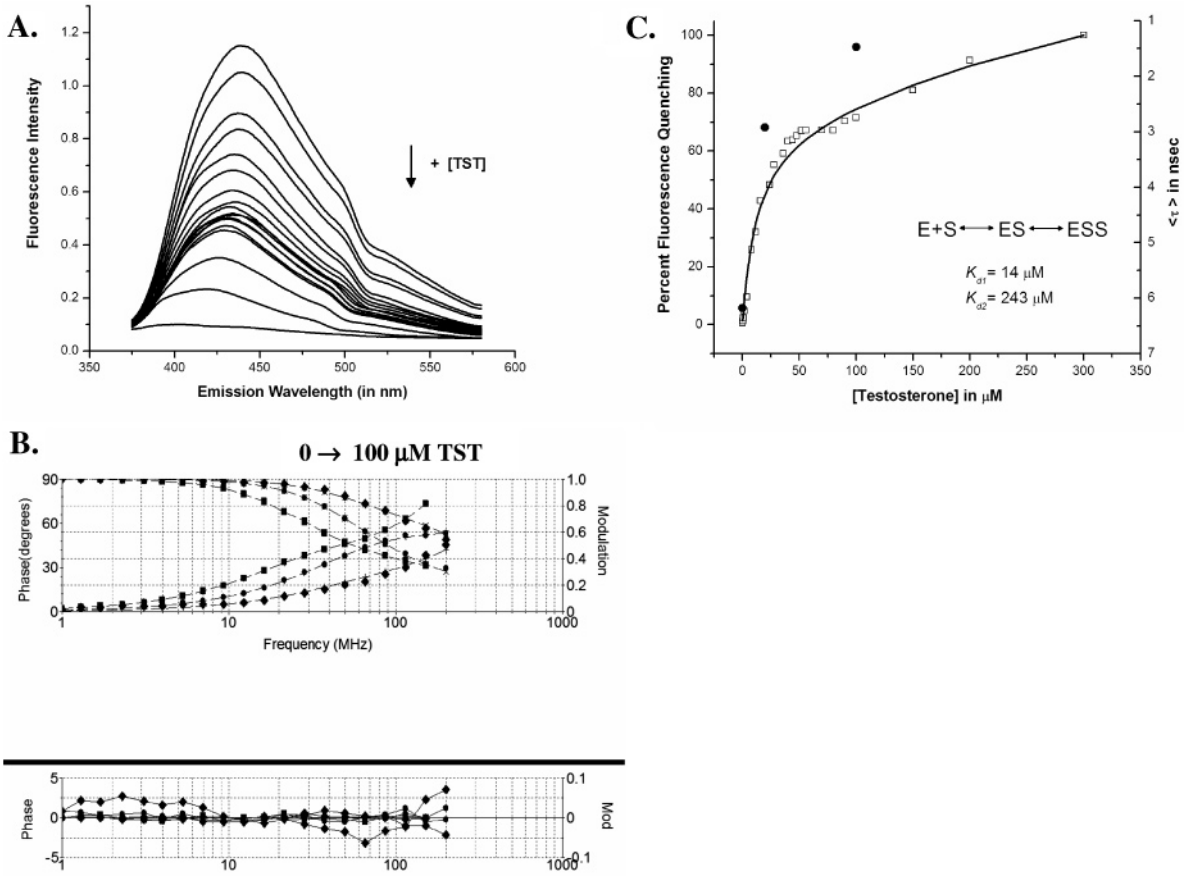

FIGURE 6: Testosterone quenches the steady-state fluorescence and decreases the fluorescence lifetime of 3 μM TNS bound to 5 μM CYP3A4. (A) Steady-state emission spectrum of TNS bound to CYP3A4 in the presence of increasing concentrations of testosterone. The testosterone concentration increases with the downward arrow. (B) Phase modulation domain decay data for emission of TNS from CYP3A4 in the presence of increasing testosterone concentrations [(■) 0, (●) 20, and (◆) 100 μM TST; λ_{ext} = 318 nm, λ_{ems} = 440 nm]. Note the clear dependence of fluorescence lifetime on TST concentration. (C) Plot of TST steady-state quenching of TNS−CYP3A4 emission (□) vs TNS average fluorescence lifetime (●) at various concentrations of TST. Steady-state quenching data were fit to eq 3 to obtain the K_d values for the first and second TST binding events.

K_d values for TST measured here are "apparent" because of the presence of ligand-free CYP3A4 in the experiment. An important feature of this fluorescence quenching curve is that the first, high-affinity, TST binding event quenches TNS fluorescence. There is no lag in the quenching versus TST concentration curve. In contrast, UV−vis difference spectra of the titration of TST into TNS-bound CYP3A4 indicate that the high-affinity TST molecule does not immediately decrease the fraction of low-spin heme (Figure 7A), as already observed for TST in the absence of a heterotropic ligand (*13*). Conversion from a low-spin [CYP3A4·TNS] complex to a high-spin [CYP3A4·TST] complex occurs only at higher TST concentrations, i.e., >100 μM (data not shown). This is similar to the lag observed in the curve of the high-spin fraction versus TST concentration published previously for CYP3A4 in the absence of TNS (*13*).

In summary, the first equivalent of TST that binds to TNS-bound CYP3A4 quenches TNS fluorescence but does not alter the TNS-dependent spin-state equilibrium. Whether 100 μM TST would be sufficient to generate a spin-state change, knowing that the first equivalent of TST does not, is considered in more detail below. The data suggest, but do not prove, that the high-affinity TST site is distinct from the TNS site and possibly modulates TNS fluorescence through long-range effects rather than through direct displacement of TNS. Furthermore, TST not only quenches the

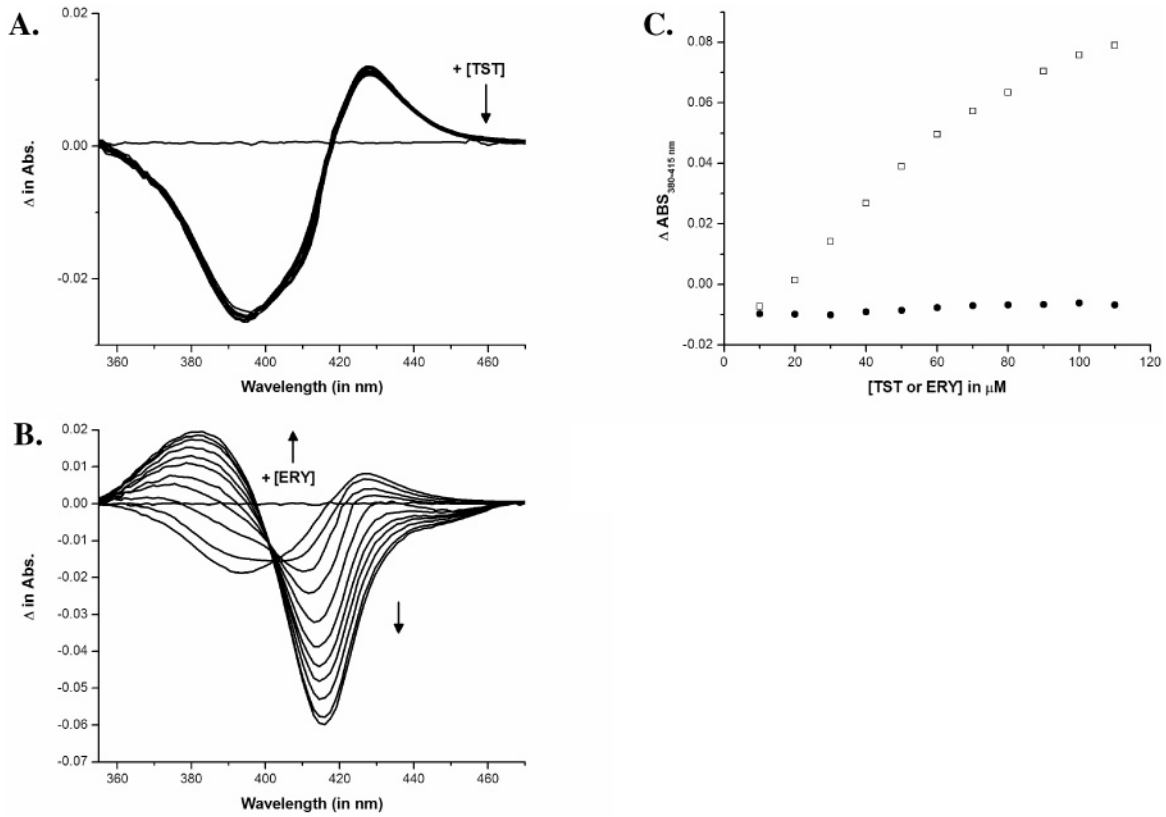

FIGURE 7: Erythromycin displaces TNS from the CYP3A4 active site, whereas testosterone does not. (A) Effect of increasing testosterone concentrations on the TNS-induced type II spin state of CYP3A4. Testosterone was titrated into the [CYP3A4·TNS] complex from 10 to 110 μM. Note that there is no substantial change in the spin state with an increase in TST concentration. (B) Effect of increasing erythromycin concentrations on the TNS-induced type II spin state. Note the conversion of the TNS-induced type II spectrum (λ_{max} = 425 nm, λ_{min} = 398 nm) to a type I spectrum (λ_{max} = 380 nm, λ_{min} = 415 nm), suggesting competitive displacement of TNS by ERY in the CYP3A4 active site. (C) Plot of the change in absorbance from 380 to 415 nm ($\Delta ABS_{380-415}$) upon addition of TST (●) or ERY (□) to the [CYP3A4·TNS] complex. Conversion from a type II spin state to a type I state occurs only upon addition of ERY and not TST.

Scheme 1: The Fluorescence Lifetime Distinguishes between Mechanisms of Heterotropic Interactions[a]

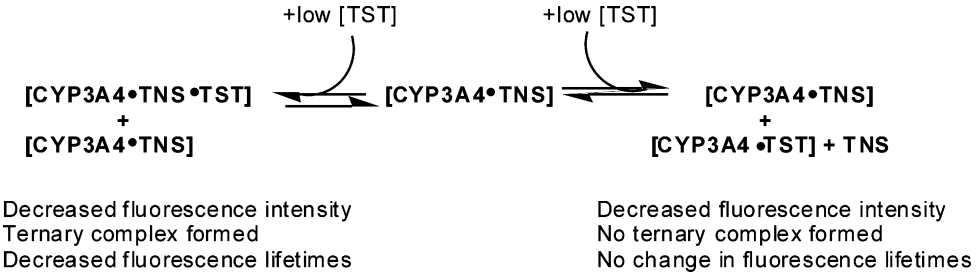

[a] If no ternary complex is formed, no change in lifetime is expected.

TNS fluorescence intensity but significantly blue shifts it as well. This directly indicates formation of a ternary [CYP3A4·TNS·TST] complex. As described below, monitoring the excited-state lifetime provides a direct probe of competitive versus noncompetitive binding for the two ligands.

If TST binds at the same site as TNS and therefore displaces it from the active site, then the apparent average lifetime of TNS will not change with an increase in TST concentration because only bound TNS contributes to the average lifetime. Displaced TNS will not be detected because it is nonfluorescent under these solution conditions. In contrast, if TST binds at a remote site or a distinct subsite within the large active site, then the decrease in steady-state fluorescence intensity will be accompanied by a decrease in excited-state lifetime. This situation is summarized in Scheme 1.

On the basis of Scheme 1, the excited-state lifetime of TNS was determined at varying TST concentrations above and below the K_d for the low-affinity TST site (Figure 6B). Higher concentrations of TST yielded poor quality phase modulation data, presumably due to the lowered fluorescent intensity of the bound TNS and the low solubility of TST. In fact, in the absence of additional cosolvent, TST begins to precipitate above 200 μM. Thus, it was technically impossible to obtain phase modulation data at high TST concentrations. However, the excited-state lifetime decreases even at low TST concentrations, and the trend is consistent with the TST concentration-dependent decrease in steady-state intensity (Figure 6C). The phase angle and modulation data clearly demonstrate a shift toward a higher-frequency response with addition of TST (Figure 6B). Interestingly, the shortest recovered lifetime contains a significant negative

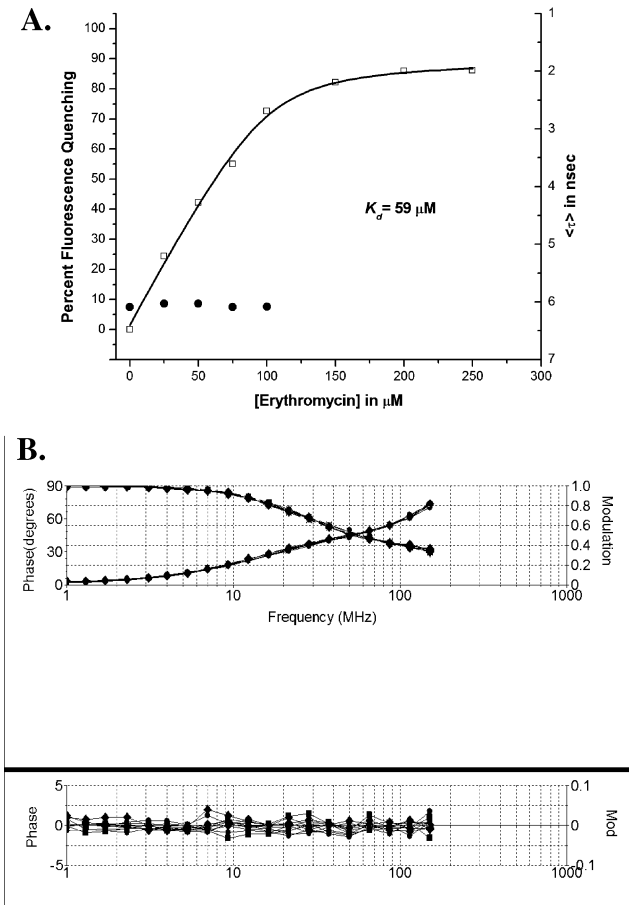

FIGURE 8: Erythromycin quenches the steady-state fluorescence of TNS bound to CYP3A4 but does not change the fluorescence lifetime. (A) Plot of ERY steady-state quenching of [TNS·CYP3A4] emission (□) vs TNS fluorescence lifetime (●) at various concentrations of ERY. Steady-state quenching data were fit to eq 2 to obtain the K_d value of ~59 μM. (B) Phase modulation decay data for emission of TNS from CYP3A4 in the presence of increasing erythromycin concentrations [(■) 0, (●) 25, (◆) 50, (▲) 75, and (▼) 100 μM ERY; λ_{ext} = 318 nm, λ_{ems} = 440 nm].

pre-exponential component, as had been seen previously with TNS bound to apomyoglobin (*25*). This negative pre-exponential component results from an excited-state reaction in which the excited-state TNS dipole experiences a change in its dipolar environment during the lifetime of the excited state (*25*), and this reaction either is too fast to observe or does not occur in the presence of TST. Regardless, TST definitely alters the excited-state dynamics or environment of TNS. Apparently, TST does not competitively displace TNS from its low-spin binding site, as suggested by the UV−vis difference spectral titration (Figure 7A). This observation is discussed further below.

To ensure that TST alone had no effect on the fluorescence lifetime of free TNS alone, TNS fluorescence lifetime measurements were recorded in the presence of 100% glycerol and 100 μM TST, in the absence of CYP3A4. No detectable change in TNS fluorescence lifetime was observed (data not shown).

For comparison, we performed the same titration experiments with ERY, which forms a high-spin heme complex. With TNS-bound CYP3A4, ERY also causes a decrease in steady-state TNS fluorescence, with an apparent K_d of ~59 μM (Figure 8A). However, in marked contrast to the TST, ERY causes no decrease in the excited-state lifetime of TNS

Scheme 2: Competitive Binding Model for TNS, ERY, and TST

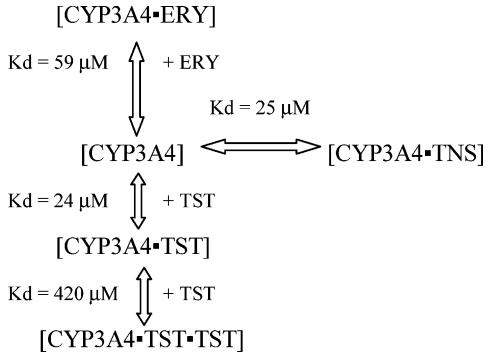

(Figure 8A,B). Thus, ERY must be competitively displacing TNS. In addition, during the optical titration experiment with ERY, a clear conversion from the TNS-induced type II spectrum (λ_{max} = 425 nm, λ_{min} = 398 nm) to a type I spectrum (λ_{max} = 380 nm, λ_{min} = 415 nm) is observed, even at low concentrations (<100 μM) of ERY, suggesting competitive displacement of TNS by ERY in the CYP3A4 active site (Figure 7B,C). These experiments provide "positive controls" for our experimental design and further demonstrate that the high-affinity TST does not compete with the TNS low-spin complex.

It is possible that TNS and each TST bind cooperatively at remote sites, affecting each other's K_d values. In fact, the data suggest that there is some positive cooperativity, inasmuch as the K_d values for TST in the absence of TNS are 22 and 440 μM (*13*) versus 14 and 243 μM in the presence of TNS. In principle, the complete free energy couplings between TNS and each TST binding are available from a comparison of each TST K_d in the presence and absence of TNS, and from the TNS K_d in the presence of one or two TST molecules. However, two aspects of the experiments prevent a full analysis of the cooperativity. (1) As noted above, the titrations with TST and ERY were performed with a subsaturating TNS concentration, and (2) we do not know the quantum yield of TNS fluorescence in the presence of one TST versus two TSTs, or the relative quenching efficiencies of each TST. However, it is useful to estimate the concentration of each species present at equilibrium in the TST−TNS competition experiment based on the true K_d' values that are experimentally available from the current work or previous work (*13*), assuming no ternary complex formation, to emphasize the correlation between the different spectral effects observed and the species present in solution. Using the true K_d values for TNS (25 μM) determined here in the absence of TST and the values for TST (22 and 440 μM) determined previously in the absence of TNS (*13*), simulations were performed to calculate the concentration of all species present at equilibrium assuming a simple competitive model (Scheme 2 and Table 3).

For the sake of completeness, the apparent K_d for ERY (59 μM), as determined by the displacement of TNS, was also used in the simulation. Previously described K_d values for binding of ERY to CYP3A4 have been reported to be somewhat lower (~52 μM) (*32*). The values in Table 3 indicate that 100 μM TST combined with a total of 5 μM CYP3A4 and 3 μM TNS is sufficient to decrease the concentration of the [CYP3A4·TNS] complex, with a type

Table 3: Equilibrium Concentrations of All Species at Varying TST Concentrations or 25 μM ERY for a Competitive Binding Mechanism (Scheme 2)[a]

predominant spin state	0 μM TST[b]	20 μM TST[b]	100 μM TST[b]	25 μM ERY[b]
[CYP3A4] low-spin, reverse type I	4.56	2.59	0.79	3.32
[TNS]	2.55	2.73	2.92	2.66
[CYP3A4·TNS] low-spin, type II	0.45	0.28	0.09	0.35
[CYP3A4·TST] low-spin, reverse type I		2.08	3.39	
[CYP3A4·TST·TST] high-spin, type I		0.08	0.73	
[CYP3A4·ERY] high-spin				1.32
[ERY]				23.7

[a] Based on 3 μM TNS total, 5 μM CYP3A4 total, a K_d for TNS of 25 μM, a K_{d1} for TST of 22 μM, and a K_{d2} for TST of 440 μM in the absence of TNS (ref *13*). [b] Initial concentration of heterotropic species.

II spectrum, from 0.45 μM in the absence of TST to 0.09 μM. Although 100 μM TST is sufficient for formation of only 0.73 μM high-spin, type I, [CYP3A4·TST·TST] complex, with a majority of 3.39 μM reverse type I [CYP3A4·TST] complex, this is accompanied by a decrease in [CYP3A4·TNS] by ~92% (from 1.46 to 0.09), in favor of [CYP3A4·TST], [CYP3A4·TST·TST], and [CYP3A4·TST·TNS]. Thus, although it is impossible to calculate exactly how large a spectral change might be expected upon addition of 100 μM TST as in Figure 7, it is very likely that some spectral change would have been observed if TST had displaced TNS. The complete absence of a spectral change under conditions that cause a clear change in fluorescence further suggests that such a competitive binding mechanism for TNS and TST is not operative. Note that similar calculations (Table 3) predict that the lowest concentration of ERY (25 μM) causes a decrease in [CYP3A4·TNS] of only ~25% and that is sufficient to cause an observable spectral change. This is consistent with a competitive ERY−TNS interaction.

A similar calculation for the noncompetitive case is not very informative for the reasons outlined above regarding the unavailability of true K_d values. However, intuitively, the major species present would be [CYP3A4·TNS·TST], which forms with a relatively high affinity based on the apparent K_d of 14 μM for TST. If, upon binding TST at a remote site, this species has a type II spectrum, then much less of the total species would be distributed to reverse type I or type I species, and a spectral change smaller than that for the competitive case is expected. Thus, the UV−vis spectral titrations do not prove a noncompetitive mechanism, but they are inconsistent with a competitive mechanism for TST and TNS. The UV−vis and fluorescence results are consistent, however.

DISCUSSION

CYP3A4 exhibits complex steady-state kinetics, in which substrate and effector concentration can influence the regioselectivity and kinetic profile of substrate oxidation (*18*, *33*, *34*). An understanding of the complex steady-state kinetics of CYP3A4 and other CYPs ultimately may require detailed knowledge of the spatial relationship between the binding sites for various ligands. For this reason, we have considered the utility of fluorescent probes in distinguishing discrete binding sites and monitoring changes in the environment of the active site when multiple ligands are bound simultaneously. Although many drugs fluoresce in aqueous solution, they are efficiently quenched upon binding to heme proteins and thus provide marginal utility as fluorescent probes (*35*, *36*). On the other hand, model compounds with other spectral properties provide a possible strategy for understanding CYP ligand dynamics.

Historically, TNS and its congener ANS have been used as probes of protein−ligand dynamics for a number of proteins, including apomyoglobin, apohemoglobin, BSA, glutamine synthetase, α1-acid glycoprotein, and RUBISCO (ribulose-1,5-bisphosphate carboxylase/oxygenase) (*23*, *24*, *37*−*39*). The primary utility of TNS and ANS lies in their tendency to exhibit only fluorescence when present in a highly hydrophobic environment, such as a lipid or the interior of proteins (*23*). Here, we have demonstrated that TNS is an excellent fluorescent probe of CYP3A4−ligand dynamics because its fluorescence is detectable only when bound to protein (Figure 4A). In addition, optical titration and kinetic inhibition studies strongly suggest its identity as a low-spin active site ligand for CYP3A4 (Figures 2 and 3). Although our data do not prove that TNS is bound in the active site, this is the most likely scenario on the basis of the numerous crystal structures of bacterial and human CYPs with ligands bound that cause type II spectral shifts, wherein the ligand forms a coordinate bond with the heme iron. There is no precedent of which we are aware in which a type II spectrum in CYP3A4 is reasonably assigned to a protein−iron coordinate bond. It is remotely possible, however, that TNS induces the spectral change and inhibition of catalytic activity from a remote binding site. If this were the case, then the data indicate that this site is distinct from the TST binding site and competitive with the ERY site. Therefore, this possibility seems unlikely. Regardless, a very clear conclusion based on these results is that the first TST is not competitive with the TNS binding, whereas ERY is.

To determine the effect that the binding of a known heterotropic effector might have on the TNS fluorescence signal, a titration with TST was conducted in both steady-state and fluorescence lifetime experiments (Figure 6). As seen in Figure 6C, both the average fluorescence lifetime of bound TNS and the magnitude of the steady-state fluorescence signal decrease at TST concentrations expected to populate the high-affinity site, but not the second low-affinity site. This is in stark contrast to the result obtained upon titrating ERY, a much larger CYP3A4 active site ligand that is not known to exhibit allosteric effects, under the same conditions. In fact, the steady-state fluorescence signal is quenched while the average fluorescence lifetime remains unchanged (Figure 8). These results demonstrate that high-affinity TST binding does not compete with TNS, which we propose is bound directly to the sixth axial heme position within the active site. The first equivalent of TST that binds

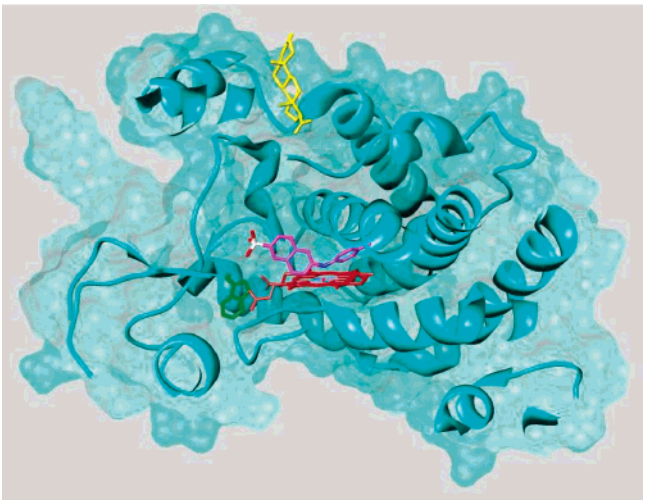

FIGURE 9: [CYP3A4·progesterone] crystal structure with TNS manually docked in the active site. Protein Data Bank entry 1WOF with progesterone bound to CYP3A4 was used to position energy-minimized TNS (magenta) in the active site with the nitrogen atom directly above the heme iron, consistent with the low-spin complex observed spectrally. Trp-126, an active site tryptophan residue, is colored green and progesterone yellow. We propose that the high-affinity TST site is the same as that of progesterone and that binding to this site modulates the excited-state properties of TNS coordinated to the heme iron.

is at a remote site, a conclusion consistent with its inability to perturb the spin state, as previously documented (*13*, *30*). We propose that the first TST binds on the periphery of CYP3A4 in an allosteric site, previously termed the "phenylalanine cluster" (*11*). Support for the existence of this binding site comes from several lines of evidence: (1) the progesterone-bound CYP3A4 crystal structure, which shows electron density for the progesterone ligand between F219 and F220, some 18 Å from the heme iron (*11*), (2) site-directed mutagenesis studies demonstrating the involvement of F213, F215, and F219 in heterotropic and homotropic cooperativity (*40*), and (3) optical spin-state titration studies that show no spin-state conversion upon the first TST binding event, consistent with TST binding at a distant allosteric site (*13*). This proposal is schematized in Figure 9.

An alternative possibility is the existence of a remote TST binding site within the CYP3A4 active site but distinct from the heme binding site. On the basis of observations from the two published crystal structures, the putative CYP3A4 active site is certainly large enough to accommodate a second ligand molecule (*10*, *11*). Further experiments should distinguish between these two possibilities, although we must point out that these possibilities are not mutually exclusive.

The TNS time-resolved fluorescence data also suggest significant changes in the dynamics of CYP3A4 when TNS binds and when TST binds to the [TNS·CYP3A4] complex. In the case of the Trp fluorescence, at least three lifetime components are required to fit the data for the unliganded protein, whereas addition of TNS results in a biexponential decay (Table 1). Although it is difficult to directly assign a physical basis for this, it is commonly observed that binding of ligands to proteins causes a general "tightening" of the structure that can reduce the number of resolvable lifetime components (*41*). Alternatively, a specific conformational change involving one of the Trp residues may occur upon binding of TNS. Further studies explicitly focused on Trp fluorescence may clarify this observation.

For the TNS fluorescence, it is striking that a negative pre-exponential term is recovered for the TNS bound to CYP3A4 and that this negative pre-exponential term is eliminated upon addition of TST. As suggested in previous studies with TNS and ANS (*25*), the negative pre-exponential term reflects an excited-state reaction in which a state initially populated upon excitation is changed to a different species before relaxing to the ground state and emitting fluorescent light. In this case, the excited-state reactions causing this negative pre-exponential term could include solvent dipole reorganization, protein−dipole interactions, or movement of the TNS probe on the time scale of the excited state. Additional experiments are required to further distinguish between these mechanisms, but these data indicate that the active site dynamics of CYP3A4 include solvent, protein, or TNS reorganization on the same time scale as the TNS lifetime (nanoseconds). Most importantly, the data further suggest that TST bound at a distinct site alters these dynamics. The dipole reorganization (negative pre-exponential) observed in the absence of TST is not observed its presence; the first equivalent of TST changes the rate at which solvent, protein residues, or TNS reorganizes within the active site. This could have implications for homotropic and heterotropic effects on absolute turnover rate, the extent of uncoupling to peroxides, and regioselectivity. For example, if solvent reorganization is responsible for the negative pre-exponential term in the TNS decay, then addition of TST with loss of the negative pre-exponential term could reflect a decreased level of hydration of the TNS, and a more "crowded" active site. In fact, this proposal is supported by the TST-induced blue shift in the spectrum of TNS, which directly indicates that TNS is in a more hydrophobic environment upon addition of TST. To our knowledge, no previous data have demonstrated a change in the dynamics of an active site CYP ligand and its environment upon occupancy of a distinct effector site. Additional fluorescence studies may further elucidate these possibilities.

In summary, we have established the utility of the solvent-quenched fluorescent probe TNS in directly monitoring protein−ligand dynamics in CYP3A4 through steady-state and time-resolved fluorescence spectroscopy. Both optical titration and metabolic inhibition demonstrate that TNS is a probable active site ligand. Recovered TNS fluorescence lifetimes in the presence of the heterotropic ligand TST suggest a peripheral allosteric binding site, consistent with previous crystallographic and thermodynamic results. Future studies utilizing this probe in conjunction with other allosteric effector−substrate combinations or protein cofactors may further elucidate the allosteric mechanisms in CYP3A4.

ACKNOWLEDGMENT

We acknowledge support of the University of Washington School of Pharmacy DMTPR Program, technical assistance from Shawna Hengel, and helpful discussions with Drs. Arthur Roberts and Michael Trnka.

REFERENCES

1. Guengerich, F. P. (2002) Cytochrome P450 enzymes in the generation of commercial products, *Nat. Rev. Drug Discovery 1*, 359−66.

2. Cupp, M. J., and Tracy, T. S. (1998) Cytochrome P450: New nomenclature and clinical implications, *Am. Fam. Physician 57*, 107−16.
3. MacCoss, M., and Baillie, T. A. (2004) Organic chemistry in drug discovery, *Science 303*, 1810−3.
4. Buening, M. K., Chang, R. L., Huang, M. T., Fortner, J. G., Wood, A. W., and Conney, A. H. (1981) Activation and inhibition of benzo[*a*]pyrene and aflatoxin B1 metabolism in human liver microsomes by naturally occurring flavonoids, *Cancer Res. 41*, 67−72.
5. Huang, M. T., Johnson, E. F., Muller-Eberhard, U., Koop, D. R., Coon, M. J., and Conney, A. H. (1981) Specificity in the activation and inhibition by flavonoids of benzo[*a*]pyrene hydroxylation by cytochrome P-450 isozymes from rabbit liver microsomes, *J. Biol. Chem. 256*, 10897−901.
6. Huang, M. T., Chang, R. L., Fortner, J. G., and Conney, A. H. (1981) Studies on the mechanism of activation of microsomal benzo[*a*]pyrene hydroxylation by flavonoids, *J. Biol. Chem. 256*, 6829−36.
7. Lasker, J. M., Huang, M. T., and Conney, A. H. (1982) In vivo activation of zoxazolamine metabolism by flavone, *Science 216*, 1419−21.
8. Johnson, E. F., Schwab, G. E., and Dieter, H. H. (1983) Allosteric regulation of the 16α-hydroxylation of progesterone as catalyzed by rabbit microsomal cytochrome P-450 3b, *J. Biol. Chem. 258*, 2785−8.
9. Korzekwa, K. R., Krishnamachary, N., Shou, M., Ogai, A., Parise, R. A., Rettie, A. E., Gonzalez, F. J., and Tracy, T. S. (1998) Evaluation of atypical cytochrome P450 kinetics with two-substrate models: Evidence that multiple substrates can simultaneously bind to cytochrome P450 active sites, *Biochemistry 37*, 4137−47.
10. Yano, J. K., Wester, M. R., Schoch, G. A., Griffin, K. J., Stout, C. D., and Johnson, E. F. (2004) The structure of human microsomal cytochrome P450 3A4 determined by X-ray crystallography to 2.05-Å resolution, *J. Biol. Chem. 279*, 38091−4.
11. Williams, P. A., Cosme, J., Vinkovic, D. M., Ward, A., Angove, H. C., Day, P. J., Vonrhein, C., Tickle, I. J., and Jhoti, H. (2004) Crystal structures of human cytochrome P450 3A4 bound to metyrapone and progesterone, *Science 305*, 683−6.
12. Shou, M., Grogan, J., Mancewicz, J. A., Krausz, K. W., Gonzalez, F. J., Gelboin, H. V., and Korzekwa, K. R. (1994) Activation of CYP3A4: Evidence for the simultaneous binding of two substrates in a cytochrome P450 active site, *Biochemistry 33*, 6450−5.
13. Roberts, A. G., Campbell, A. P., and Atkins, W. M. (2005) The thermodynamic landscape of testosterone binding to cytochrome P450 3A4: Ligand binding and spin state equilibria, *Biochemistry 44*, 1353−66.
14. Gillam, E. M., Baba, T., Kim, B. R., Ohmori, S., and Guengerich, F. P. (1993) Expression of modified human cytochrome P450 3A4 in *Escherichia coli* and purification and reconstitution of the enzyme, *Arch. Biochem. Biophys. 305*, 123−31.
15. Omura, T., and Sato, R. (1962) A new cytochrome in liver microsomes, *J. Biol. Chem. 237*, 1375−6.
16. Cheng, Y., and Prusoff, W. H. (1973) Relationship between the inhibition constant (K1) and the concentration of inhibitor which causes 50% inhibition (I50) of an enzymatic reaction, *Biochem. Pharmacol. 22*, 3099−108.
17. Shaw, P. M., Hosea, N. A., Thompson, D. V., Lenius, J. M., and Guengerich, F. P. (1997) Reconstitution premixes for assays using purified recombinant human cytochrome P450, NADPH-cytochrome P450 reductase, and cytochrome b5, *Arch. Biochem. Biophys. 348*, 107−15.
18. Lu, P., Lin, Y., Rodrigues, A. D., Rushmore, T. H., Baillie, T. A., and Shou, M. (2001) Testosterone, 7-benzyloxyquinoline, and 7-benzyloxy-4-trifluoromethyl-coumarin bind to different domains within the active site of cytochrome P450 3A4, *Drug Metab. Dispos. 29*, 1473−9.
19. Lakowicz, J. R., Cherek, H., and Balter, A. (1981) Correction of timing errors in photomultiplier tubes used in phase-modulation fluorometry, *J. Biochem. Biophys. Methods 5*, 131−46.
20. Mendes, P. (1993) GEPASI: A software package for modelling the dynamics, steady states and control of biochemical and other systems, *Comput. Appl. Biosci. 9*, 563−71.
21. Mendes, P. (1997) Biochemistry by numbers: Simulation of biochemical pathways with Gepasi 3, *Trends Biochem. Sci. 22*, 361−3.
22. Mendes, P., and Kell, D. (1998) Non-linear optimization of biochemical pathways: Applications to metabolic engineering and parameter estimation, *Bioinformatics 14*, 869−83.
23. Stryer, L. (1965) The interaction of a naphthalene dye with apomyoglobin and apohemoglobin. A fluorescent probe of non-polar binding sites, *J. Mol. Biol. 13*, 482−95.
24. McClure, W. O., and Edelman, G. M. (1966) Fluorescent probes for conformational states of proteins. I. Mechanism of fluorescence of 2-p-toluidinylnaphthalene-6-sulfonate, a hydrophobic probe, *Biochemistry 5*, 1908−19.
25. Lakowicz, J. R., Gratton, E., Cherek, H., Maliwal, B. P., and Laczko, G. (1984) Determination of time-resolved fluorescence emission spectra and anisotropies of a fluorophore-protein complex using frequency-domain phase-modulation fluorometry, *J. Biol. Chem. 259*, 10967−72.
26. Bismuto, E., Sirangelo, I., and Irace, G. (1989) Conformational substates of myoglobin detected by extrinsic dynamic fluorescence studies, *Biochemistry 28*, 7542−5.
27. Atkins, W. M. (2005) Non-Michaelis−Menten kinetics in cytochrome P450-catalyzed reactions, *Annu. Rev. Pharmacol. Toxicol. 45*, 291−310.
28. Domanski, T. L., Liu, J., Harlow, G. R., and Halpert, J. R. (1998) Analysis of four residues within substrate recognition site 4 of human cytochrome P450 3A4: Role in steroid hydroxylase activity and α-naphthoflavone stimulation, *Arch. Biochem. Biophys. 350*, 223−32.
29. Andrews, J., Abd-Ellah, M. F., Randolph, N. L., Kenworthy, K. E., Carlile, D. J., Friedberg, T., and Houston, J. B. (2002) Comparative study of the metabolism of drug substrates by human cytochrome P450 3A4 expressed in bacterial, yeast and human lymphoblastoid cells, *Xenobiotica 32*, 937−47.
30. Baas, B. J., Denisov, I. G., and Sligar, S. G. (2004) Homotropic cooperativity of monomeric cytochrome P450 3A4 in a nanoscale native bilayer environment, *Arch. Biochem. Biophys. 430*, 218−28.
31. Yoon, M. Y., Campbell, A. P., and Atkins, W. M. (2004) "Allosterism" in the elementary steps of the cytochrome P450 reaction cycle, *Drug Metab. Rev. 36*, 219−30.
32. McConn, D. J., II, Lin, Y. S., Allen, K., Kunze, K. L., and Thummel, K. E. (2004) Differences in the inhibition of cytochromes P450 3A4 and 3A5 by metabolite-inhibitor complex-forming drugs, *Drug Metab. Dispos. 32*, 1083−91.
33. Shou, M., Dai, R., Cui, D., Korzekwa, K. R., Baillie, T. A., and Rushmore, T. H. (2001) A kinetic model for the metabolic interaction of two substrates at the active site of cytochrome P450 3A4, *J. Biol. Chem. 276*, 2256−62.
34. Khan, K. K., He, Y. Q., Domanski, T. L., and Halpert, J. R. (2002) Midazolam oxidation by cytochrome P450 3A4 and active-site mutants: An evaluation of multiple binding sites and of the metabolic pathway that leads to enzyme inactivation, *Mol. Pharmacol. 61*, 495−506.
35. Stortelder, A., Keizers, P. H., Oostenbrink, C., de Graaf, C., de Kruijf, P., Vermeulen, N. P., Gooijer, C., Commandeur, J. N., and van der Zwan, G. (2005) Binding of 7-methoxy-4-(aminomethyl)-coumarin to wild-type and W128F mutant cytochrome P450 2D6 studied by time-resolved fluorescence spectroscopy, *Biochem. J. 393* (Pt 3), 635−43.
36. Shumyantseva, V. V., Bulko, T. V., Petushkova, N. A., Samenkova, N. F., Kuznetsova, G. P., and Archakov, A. I. (2004) Fluorescent assay for riboflavin binding to cytochrome P450 2B4, *J. Inorg. Biochem. 98*, 365−70.
37. Albani, J. (1992) Motions studies of the human α1-acid glycoprotein (orosomucoid) followed by red-edge excitation spectra and polarization of 2-p-toluidinylnaphthalene-6-sulfonate (TNS) and of tryptophan residues, *Biophys. Chem. 44*, 129−37.
38. Lin, W. Y., Eads, C. D., and Villafranca, J. J. (1991) Fluorescent probes for measuring the binding constants and distances between the metal ions bound to *Escherichia coli* glutamine synthetase, *Biochemistry 30*, 3421−6.
39. Frank, J., Holzwarth, J. F., Hoek, A. V., Visser, A. J. W. G., and Vater, J. (1997) Kinetics and equilibrium binding of the dyes TNS and RH421 to rubulose 1,5-bisphosphate carboxylase/oxygenase (RUBISCO), *J. Chem. Soc., Faraday Trans. 93*, 2379−85.

40. Harlow, G. R., and Halpert, J. R. (1998) Analysis of human cytochrome P450 3A4 cooperativity: Construction and characterization of a site-directed mutant that displays hyperbolic steroid hydroxylation kinetics, *Proc. Natl. Acad. Sci. U.S.A. 95*, 6636−41.

41. Atkins, W. M., Stayton, P. S., and Villafranca, J. J. (1991) Time-resolved fluorescence studies of genetically engineered *Escherichia coli* glutamine synthetase. Effects of ATP on the tryptophan-57 loop, *Biochemistry 30*, 3406−16.

BI060083H